AAPS Introductions in the Pharmaceutical Sciences

Dimitrios A. Lamprou
Edward Weaver *Editors*

Microfluidics in Pharmaceutical Sciences

Formulation, Drug Delivery, Screening, and Diagnostics

aaps®

Springer

AAPS Introductions in the Pharmaceutical Sciences

Volume 14

The *AAPS Introductions in the Pharmaceutical Sciences* book series is designed to support pharmaceutical scientists at the point of knowledge transition. Springer and the American Association of Pharmaceutical Scientists (AAPS) have partnered again to produce a second series that juxtaposes the *AAPS Advances in the Pharmaceutical Sciences* series. Whether shifting between positions, business models, research project objectives, or at a crossroad in professional development, scientists need to retool to meet the needs of the new scientific challenges ahead of them. These educational pivot points require the learner to develop new vocabulary in order to effectively communicate across disciplines, appreciate historical evolution within the knowledge area with the aim of appreciating the current limitations and potential for growth, learn new skills and evaluation metrics so that project planning and subsequent evolution are evidence-based, as well as to simply "dust the rust off" content learned in previous educational or employment settings, or utilized during former scientific explorations. The *Introductions* book series will meet these needs and serve as a quick and easy-to-digest resource for contemporary science.

Dimitrios A. Lamprou • Edward Weaver
Editors

Microfluidics in Pharmaceutical Sciences

Formulation, Drug Delivery, Screening, and Diagnostics

Springer

aaps®

Editors
Dimitrios A. Lamprou
School of Pharmacy
Queen's University Belfast
Belfast, UK

Edward Weaver
School of Pharmacy
Queen's University Belfast
Belfast, UK

ISSN 2522-834X ISSN 2522-8358 (electronic)
AAPS Introductions in the Pharmaceutical Sciences
ISBN 978-3-031-60716-5 ISBN 978-3-031-60717-2 (eBook)
https://doi.org/10.1007/978-3-031-60717-2

This Springer imprint is published by the registered company Springer Nature Switzerland AG
The registered company address is: Gewerbestrasse 11, 6330 Cham, Switzerland

Preface

This book, titled *Fundamentals and Prospects of Microfluidics in Pharmaceutical Sciences: From formulation to Drug Delivery, Screening, and Diagnostics*, covers a broad spectrum of applications posed by the emerging technology of microfluidics. Over 18 separate chapters written by experts across the world, readers can expect to find information relating to key utilisations which relate to their use for pharmaceutical manufacturing and medicinal practice. The book initially looks into the use of microfluidics for nanofabrication purposes due to its broad capacity for the production of nanomedicines and medical devices, before moving onto the use of microfluidics for other uses such as diagnostics and gene therapy. The book concludes by investigating near-future and far-future promises of microfluidics such as scalability and the introduction of artificial intelligence.

Each chapter is additionally equipped with a multiple-choice question section, which will allow the reader to examine their understanding of the content of the chapter and identify areas of improvement.

The introductory chapter covers the basic principles of microfluidics, highlighting aspects of the technology such as fluid flow and miniaturisation, as well as introducing some of the most important equations that underpin microfluidic functionality such as Navier-Stokes, diffusion and mixing. This chapter aims to enhance the readers of the potential that microfluidics has to offer, before delving into specific applications later throughout the book.

Chapter 2 covers an important aspect of all pharmaceutical processes, especially microfluidics: sustainability. The chapter assesses how microfluidics is being used sustainably and how its practices can be improved. Instead of focussing on progressing microfluidics as rapidly as possible, this chapter investigates how a similar standard of process can be achieved in a more sustainable fashion.

The fabrication of lipid-based nanoformulations is key application that is becoming optimised via a microfluidic method; hence, Chap. 3 explores this concept for the formulation of liposomes. From flow parameters, lipid choices, payload capacity and comparisons with previously established methods of liposomal fabrication, a diverse range of topics are explored and explained. Common characterisation

techniques for lipid nanoformulations, e.g. dynamic light scattering, are mentioned, especially with regard to their advantages and drawbacks.

Following on from the microfluidic production of liposomes, the concept of niosome fabrication is examined in the next chapter. So called due to their composition from non-ionic surfactants, niosomes offer a high propensity for both therapeutic treatment and diagnostic potential. Their manufacturing is discussed in detail, as well as exploring their customisation, drug delivery applications and methods of teaching.

Continuing the nanoparticle theme, polymeric nanoparticles are discussed; thoroughly investigating their pharmaceutical applications. Since their manufacturing route is altered as compared to lipid-based nanoparticles, the microfluidic conditions must be altered to allow for their successful formulation. From polysaccharides to synthetic polymers, a broad range of polymeric nanoparticles are covered in this chapter, further highlighting the scope of microfluidics for unique applications.

Inorganic nanoparticles and nanomaterials such as silicon or metal composites are a key area to mention due to their theranostic pharmaceutical applications. Additionally, with the rising use of quantum dot technology, an efficient synthesis route must be realised. In this chapter, all these factors are addressed in a concise manner, with gaps in literature and promising aspects of the technology being identified.

The use of carbon-based nanomaterials is investigated in Chap. 7, drawing from a wealth of promising research currently being undertaken in this area. Aspects such as carbon and graphene dot on-chip synthesis, as well as integrated hybrid nanomaterial fabrication, are discussed, especially relating to topics such as drug delivery and biosensing.

Gene delivery is touched upon in the following chapter, highlighting the potential and current uses of this cutting-edge technology. Specific focuses on Chimeric Antigen Receptor (CAR) T-cell therapy and viral/nonviral vectors are investigated here in relation to cell and gene therapy. The chapter addresses the important technique of electroporation, a permeabilization technique for cell membranes, which has been shown to have key microfluidic applications.

Flow cytometry, a technique involved in the analysis of cells and particles, is extremely amenable to microfluidic applications. General applications of the technology are discussed, before delving deeper into aspects such as cell focusing, imaging and the application of machine learning. The promising use of microfluidics for flow cytometry are constantly evolving, making it an important application to observe for future developments.

Chapter 10 looks into how microfluidics can offer point-of-care viability, helping ensure that populations across the world may have access to this technology. Used mainly for diagnostic applications, point-of-care microfluidic devices allow a portable solution to various disease-state identification, such as cancer and pathogenic infection.

The treatment and diagnosis of cancer has been a constant battle for decades, and microfluidics has begun to have a positive impact upon this task. This chapter probes

into the current state of oncologic treatment, from nanoparticles to drug discovery, as well as appraising how cancer can be diagnosed and monitored using this emerging technology. A thorough literature review is performed in this chapter.

Drug development is a constant challenge, owing to the continuous need to discover and produce new medicines to help combat a forever-changing medical scope. Pertinent applications of microfluidics, including organ simulations, droplet microfluidics and single-cell assays, are just a few mechanisms discussed relating to drug discovery in this chapter. The concept of microreactors is also explored, opening the pharmaceutical doorway to chemical and biological amelioration.

Microfluidics opens the possibility for precise drug delivery, which is why a focus is given to this in the following chapter. Difficult-to-treat areas such as the brain, central nervous system and transdermal delivery are discussed here in relation to their solutions using microfluidics. Utilising precise targeted delivery, off-target effects may be reduced, as well as the potential to reduce the dose required for therapeutic administration.

The area of food and nutrition is important within the pharmaceutical industry amongst others. Microfluidics offers the opportunity to enhance food safety, detect foodborne pathogens and also encapsulate bioactive compounds within nanoformulations. These factors can help contribute to the positive impact that research within food and nutrition can exhibit. Within this chapter, an extensive review on current and future applications of microfluidics within this domain is performed.

Coming towards the latter chapters of the book, a focus upon biosensors is then applied in the next chapter. Biosensors are an integral functionality of many microfluidic devices and are involved in the detection of various substances including monosaccharides and protein biomarkers. Additionally, within this chapter, the classification of biosensors is discussed, as well as the process of computationally analysing microfluidic flow.

The scalability of microfluidics is often a challenge presented when a microfluidic process is successful enough to reach industrial implementation. Chapter 16 mentions some of the key factors that need to be addressed to allow for this, including “scale-up” and “scale-out” approaches. The chapter looks at nanomedicines that already have market approval, and how their production has been scaled to an industrial level, before moving onto various alternative scaling strategies.

To ensure novelty of research being performed, the penultimate chapter explores currently active patents in the field of microfluidics. Reviewing these may help the reader identify gaps in the market, as well as introducing concepts that have assisted previous work in being successfully patented.

In the final chapter, a concise review as to the current and future perspectives of microfluidics is highlighted. The rapid growth of microfluidics, as well as the parallel growth of related technologies, has rendered a huge potential for further advancements for microfluidics. Concepts such as microfluidic normalisation, implementation of artificial intelligence and future pandemics are examples of topics covered.

The editors hope that readers find the information contained within this book useful, with the aim of inspiring the further use and development of microfluidics in the future. The knowledge contained within the chapters is pooled from a diverse range of experts from across the globe and we encourage readers to contact authors directly should they wish to discover more.

Belfast, UK

Dimitrios A. Lamprou
Edward Weaver

Contents

About the Editors

Dimitrios A. Lamprou (PhD, MBA) is the Chair of Biofabrication and Advanced Manufacturing at Queen's University Belfast. Currently, he is the author of over 160 peer-reviewed publications, has over 450 conference abstracts and has given over 180 Invited Talks in institutions and conferences across the world. PubMed-based algorithms placed Prof. Lamprou in the top 0.07% of scholars in the world writing about microfluidics, in the past 10 years. Prof. Lamprou has also been named in the Stanford University's list of World's Top 2% Scientists, for several consecutive years, for his research in Pharmaceutics and Biomedical Engineering.

Edward Weaver (PhD, MPharm) completed his degree in Pharmacy, at the University of Nottingham, before pursuing a PhD at Queen's University Belfast. His doctorate research focussed on the sustainable microfluidic production of lipid nanoparticles, with a specific focus up the encapsulation of biologics. During his academic career, Edward has published over 20 manuscripts and has attended multiple conferences to showcase his work. He has a focus upon industrial scalability of various pharmaceutical media and is currently working upon improving scalable downstream manufacturing systems.

Basic Principles of Microfluidics

Pedro Fernandes

Abstract Microfluidics is a rapidly evolving multidisciplinary field that relies on the manipulation of minute volumes of fluids in submillimeter-sized channels with application in chemistry, biotechnology, and health, among other relevant areas. At this scale, a paradigm shift takes place, as phenomena that are unnoticed at the macroscale emerge, since viscous, capillary, and surface tension effects tend to overcome gravity and inertial effects. Therefore, flow behavior often contradicts our macroscopic intuition, yet may easily become more predictable and thus controllable. This chapter focuses on the physics aspects underlying microfluidics. Thus, the basics of fluid mechanics are introduced and the governing equations for fluid flow are presented. Mass transfer and in particular diffusion and diffusion advection aspect are introduced and discussed and complemented with a brief incursion in the strategies for mixing at the microscale, developed to overcome the limitations of diffusion-based processes. Surface tension and capillarity effects are described and their significance in microfluidics is elucidated, also considering their impact in droplets/bubbles formation and multiphase flow.

Keywords Miniaturization · Fluid dynamics · Mass transfer · Micromixing · Surface tension

P. Fernandes (✉)
Faculdade de Engenharia, Universidade Lusófona, Lisbon, Portugal

iBB—Institute for Bioengineering and Biosciences, Instituto Superior Técnico, Universidade de Lisboa, Lisbon, Portugal

Associate Laboratory i4HB—Institute for Health and Bioeconomy at Instituto Superior Técnico, Universidade de Lisboa, Lisbon, Portugal
e-mail: p980@ulusofona.pt

D. A. Lamprou, E. Weaver (eds.), *Microfluidics in Pharmaceutical Sciences*,
AAPS Introductions in the Pharmaceutical Sciences 14,
https://doi.org/10.1007/978-3-031-60717-2_1

1 Introduction and Historic Perspective

Microfluidics merges the science that studies the behavior of small amounts of fluids (10^{-6}–10^{-18} L scale) in tiny channels (width or height or diameter, the so-called characteristic dimension) of tens to hundreds of micrometers [1, 2] (or in a broader perspective within 0.1 μm to 1 mm [3]), with the technology to manufacture the devices where the fluids are contained and flow [1, 2, 4, 5]. By definition, a fluid is a substance that continuously deforms (or flows) under applied shear stress, as illustrated in Fig. 1.

Microfluidics is a multidisciplinary field at the crossroads of biology, chemistry, engineering, and physics that has contributed with significant applications and innovations, namely in biochemical engineering [6, 7], analytics [8], and medical sciences [9]. Microfluidics is notoriously rooted in the microelectronics industry [10], but the efforts to understand the behavior of small amounts of fluid can be traced back to the eighteenth and nineteenth centuries [4]. From these pioneering works emerged major contributions, such as the well-known Hagen Poiseuille equation (Eq. 1). The latter estimates the pressure drop (ΔP) in a Newtonian fluid with viscosity μ that flows in a laminar way with a given volumetric flow rate (Q) in a cylindrical, horizontal pipe of radius R and length L [11, 12].

$$Q = \frac{\Delta P \pi R^4}{8 \mu L} \tag{1}$$

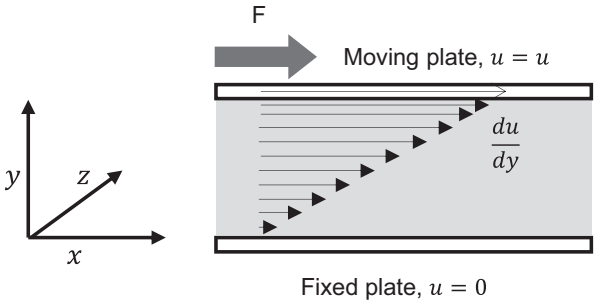

Fig. 1 Characteristic behavior of a Newtonian fluid contained within two plates at steady state. The fluid s idealized in the form of adjacent, parallel layers. The lower plate is fixed, whereas the top plate moves in one direction (x) at a fixed velocity u due to a force F applied over the entire surface of the plate A, originating shear stress, τ ($F/A = \tau$). Under the action of this force, the fluid deforms continuously. Friction between the moving plate and the fluid sets the latter in motion but as one moves away from the top layer, the adjacent fluid layers depict and increasingly lower velocity along the y axis, concomitant with a velocity gradient, du/dy, also termed shear rate. This gradient due to the viscosity of the fluid, μ, which features the fluid's ability to oppose the progress of shear deformation. Thus, for fluids, τ depends on shear rate (in solids τ depends on shear). For a Newtonian fluid, τ and shear rate are related by $\tau = -\mu(du/dy)/dt$

Additionally, Eq. 1 provides an analytical solution for the Navier-Stokes equations, a set of tridimensional nonlinear partial differential equations, based on Newton's second law (conservation of momentum), that describe the motion of viscous fluids [5, 13]. In vector notation, Navier-Stokes equations are combined as depicted in Eq. 2 for an incompressible Newtonian fluid with constant viscosity, where velocity ($\boldsymbol{u}$) vector and pressure are related and time (t) density (ρ) and gravity acceleration ($\boldsymbol{g}$) are considered [5, 12, 13]:

$$\rho \frac{\partial \boldsymbol{u}}{\partial t} + \rho\left(\boldsymbol{u} \cdot \nabla \boldsymbol{u}\right) = -\nabla \mathrm{P} + \mu \nabla^2 \boldsymbol{u} + \rho \boldsymbol{g} \tag{2}$$

where ∇ is the gradient operator, e.g., in the case of cartesian coordinates, (x, y, z) stands for $(\partial/\partial x, \partial/\partial y, \partial/\partial z)$, and for cylindrical coordinates, (r, φ, z) stands for $\left(\partial/\partial r, \frac{1}{r}\partial/\partial\theta, \partial/\partial z\right)$. Here, $\rho \frac{\partial \boldsymbol{u}}{\partial t}$ stands for accumulation of momentum, $\rho(\boldsymbol{u} \cdot \nabla \boldsymbol{u})$ stands for momentum in and out of a volume element (inertia term), and $\nabla \mathrm{P}$, $\mu \nabla^2 \boldsymbol{u}$, and $\rho \boldsymbol{g}$ stand for pressure, viscous, and gravity forces. Despite the mathematical complexity, Eq. 2 simply states that the momentum rate of change with time of a fluid element matches all the forces acting on that fluid element [5, 12]. The interested reader may gain more insight on the Navier-Stokes equation elsewhere [14–16]. In the detailed characterization of flow, Navier-Stokes equations are typically associated with the continuity equation (Eq. 3), which establishes mass conservation in fluid flow and can be simplified (Eq. 4) in the case of incompressible fluids, since density is constant over time.

$$\frac{\partial \rho}{\partial t} + \nabla\left(\rho \cdot \boldsymbol{u}\right) = 0 \tag{3}$$

$$\nabla \cdot \boldsymbol{u} = 0 \tag{4}$$

This theoretical background was to become quite useful to model and predict the behavior of fluids moving/contained within microfluidic devices. These have as distinctive feature the incorporation of channels where at least one dimension, typically the hydraulic diameter, is in the range of tens to hundreds of micrometers [17–20]. The dissemination of microfluidic devices owes significantly to the concept of "miniaturized Total Analysis System" (μTAS) that emerged in the 1990s and fostered the integration of sampling, transport of the sample, sample preparation steps if needed, and detection in a single platform with microfluidic features and where all actions are performed automatically [10, 21]. The developments associated also demonstrated that similarly to microelectronics, where the assembly of capacitors, diodes, resistors, and transistors in a single platform with a small footprint to yield an integrated circuit (or chip or microchip) was introduced in the 1960s [22], a lab-on-a-chip framework, that enclosed the features of a laboratory in a single miniaturized platform for application in different areas, e.g., (bio)medical, (bio)chemical and environmental engineering was feasible [23, 24]. Further details on the specific peculiarities of μTAS and lab-on-a-chip can be found elsewhere [25].

2 The Essence of Miniaturization

Miniaturization associated with microfluidics comes along with several advantages, namely, the small volumes involved and concomitantly lower costs with consumables; improved mass and heat transfer; high surface area-to-volume ratio (up to e.g., 5.0×10^4 m^2/m^3); improved capacity by parallelization; lower risks of contamination; enhanced sensitivity and specificity; ease of automation; precise fluid flow characterization (due to, e.g., operation at low Reynolds number, Re); possible sensor integration; and small footprint (e.g., the size of a microscope slide or of a credit card, where one to several microchannels are molded or engraved). However, there are some drawbacks associated with microfluidic devices, most notably the complexity on the manufacturing procedure (particularly when a novel structure is intended); the intricate fluidic network; the challenging integration of different components and functionalities, e.g., sensors and actuators; material compatibility, as there is no single material for manufacturing microfluidic devices that fits all applications; and the risk of channel clogging [2, 26–31].

Although often associated with analytical and early process development roles, the use of miniaturized integrated devices has moved out of the lab into preparative and production scales [32–34]. Still, given the low throughputs of microfluidic devices, the successful implementation of this strategy relies on either numbering-up or scale-out to achieve the intended throughput. The former involves the implementation of a network of similarly sized microfluidic devices operating in parallel, which rules out the requirement of complex scale-up procedures but significantly increases online monitoring and fluidic complexity (e.g., multiplicity of pumps and connectors); scale-out, on the other hand, involves the use of devices with increased dimensions, e.g. length or size, so that the characteristic dimension is likely shifted to the mm scale, which can be termed as a meso-scale [26, 34]. Although this implies poorer heat and mass transfer, surface area-to-volume ratio (e.g., upper limit $\sim 1.0 \times 10^4$ m^2/m^3), and fluid flow control and predictability when compared to typical microfluidic devices, the simplicity and diversity of design favor the scale-out strategy for scale-up [34].

3 Miniaturization and Fluid Dynamics

Given the small volumes in microfluidics, fluids behave differently than in the macroworld. Although the physical laws in the system remain unaltered, phenomena that are not apparent at larger scales gain relevance. This becomes evident once the concept of scaling laws is introduced. This concept establishes the effect of size (l) variations on given physical quantities, while other parameters, such as temperature or pressure, remain unaltered [35, 36]. To illustrate this, one can consider a system with a characteristic dimension l, then the surface area is given by l^2 and volume by

l^3. Surface forces, like capillarity, surface tension, or viscosity, relate to surface area, whereas volume forces, like inertia or weight, relate to volume. The ratio of these two forces is given by Eq. 5.

$$\frac{\text{Surface forces}}{\text{Volume forces}} \alpha \frac{l^2}{l^3} = \frac{1}{l} \tag{5}$$

In a microfluidic system, $\to 0, \text{thus} \frac{1}{l} \to \infty$; therefore, surface forces gain prominence over volume forces, unlike what is observed in our macroscopic daily life [5, 36]. One of the most immediate outcomes of this paradigm shift is flow regime in microfluidics, as predicted by the Reynolds number (*Re*) that relates the effect of inertial forces ($\rho u^2 l$) to viscous forces (μu) (Eq. 6) [2, 25, 37, 38].

$$\text{Re} = \frac{\rho u l}{\mu} = \frac{u l}{\nu} = \frac{\text{inertial forces}}{\text{viscous forces}} \tag{6}$$

where u is the linear velocity, ν is the kinematic viscosity, and l (a characteristic dimension) stands for the diameter (for flow inside a channel with cylindrical circular cross section) or for the hydraulic diameter, d_h, in the case of non-circular cross section channels (Eq. 7).

$$d_h = \frac{4A}{P} \tag{7}$$

where A is cross-sectional flow area and P is the wetted perimeter of the channel, which refers to the perimeter that contacts the fluid [37, 38].

For *Re* under ~ 1800 to 2300, flow is laminar, whereas for Re exceeding ~1800 to 2300, turbulent flow emerges [2, 39, 40]. The transition from turbulent to laminar flow that occurs at *Re*~2000 holds irrespectively of the scale [41]. Given the small dimensions in microfluidics, viscous forces are dominant; hence, small Reynolds numbers, often under 1, are observed, and laminar flow becomes dominant [25]. Therefore, smooth, steady regular streamlines and predictable flow patterns are observed, as opposite to the chaotic and unpredictable pattern observed in turbulent flow, due to changes in velocity (Fig. 2) [2, 25]. Thus, pressure-driven steady-state laminar flow of a Newtonian fluid can be described by Eq. 1 [2].

Moreover, under these conditions, the Navier-Stokes equation can be simplified and in the specific common case of flow in a cylindrical microchannel (cylindrical coordinates: r, θ, z) depicted as Eq. 8.

$$\frac{\partial p}{\partial z} = \mu \frac{1}{r} \frac{\partial}{\partial r} \left(r \frac{\partial u_z}{\partial r} \right) \tag{8}$$

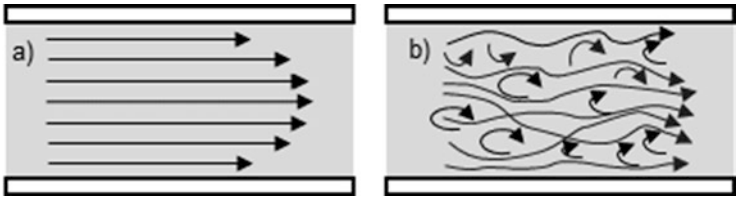

Fig. 2 Flow patterns in a channel: (**a**) laminar flow, characterized by fluids layers moving in parallel, perpendicularly to the cross section of the channel, represented by smooth streamlines that do not cross; thus, there is no lateral mixing. A viscous fluid is depicted, and hence there is a velocity gradient from the centerline of the channel (where velocity is maximal) to the walls, where velocity is nihil (assuming no-slip condition), leading to a parabolic profile; (**b**) turbulent flow, where although the bulk fluid slides in a particular direction, there are random variations of velocity and erratic flow behavior, leading to the formation of eddies and swirls, which favors mixing

This upon integration of a microchannel of length L and radius R yields Eq. 9

$$u_z = \frac{\Delta p}{L}\frac{R^2}{4\mu}\left[1-\left(\frac{r}{R}\right)^2\right] \tag{9}$$

and corresponds to a parabolic velocity profile where velocity u_z peaks at the center of the channel; hence, $u_{z,\max} = \frac{\Delta p}{L}\frac{R^2}{4\mu}$, where the frictional effect of the channel wall is most afar [2]. An average velocity can be defined as $u_{z,av} = \frac{Q}{A}$. For a rectangular cross section microchannel, where often a high aspect ratio is observed, the channel with height H can be depicted as an infinite parallel plate configuration [36, 42]. For flow in a xy plane, the velocity profile is given by Eq. 10, again a parabola:

$$u_x = \frac{\Delta p}{\mu L}(H-y)y \tag{10}$$

where again the velocity peaks at the centerline, $y = \frac{H}{2}$, hence $u_{x,\max} = \frac{\Delta p}{L}\frac{H^2}{8\mu}$ and the flow rate through a channel of width W is given by Eq. 11 [36]:

$$Q = \frac{\Delta p H^3 W}{12\mu L} \tag{11}$$

A rather common microchannel configuration in microfluidic devices is that of a rectangular cross section, with width W and height H [5, 36]. In this case, the velocity profile in Poiseuille flow is given by Eq. 12 [2, 5, 36].

$$u_x = \frac{4H^2\Delta p}{\pi^3 \mu L}\sum_{n,\text{odd}}^{\infty}\frac{1}{n^3}\left[1-\frac{\cos h\left(\frac{n\pi y}{H}\right)}{\cos h\left(\frac{n\pi W}{2H}\right)}\right]\sin\left(\frac{n\pi z}{H}\right) \tag{12}$$

and the flow rate by Eq. 13 [5, 36].

$$Q = \frac{H^3 W\Delta p}{12\mu L}\left[1-\sum_{n,\text{odd}}^{\infty}\frac{192H}{n^5\pi^5 W}\tan h\left(\frac{n\pi W}{2H}\right)\right] \tag{13}$$

which, for a flat and wide channel, hence $\frac{H}{W}\to 0$, Eq. 13 can be simplified to Eq. 14 [5, 36].

$$Q \approx \frac{H^3 W\Delta p}{12\mu L}\left(1-\frac{0.63H}{W}\right) \tag{14}$$

Further detail on velocity profiles and flow rate quantification in microchannels with other cross sections can be found elsewhere [5, 36, 43]. The use of Eqs. (8), (9), (10), (11), (12), (13) and (14) is particularly accurate for low *Re*, namely *Re* <1. Under this threshold, where conventional microfluidics is mostly operated [44, 45], the inertia term $\rho(\boldsymbol{u}\cdot\nabla\boldsymbol{u})$ in the Navier-Stokes equations can be fully neglected, leading to Eq. 15, the linear Stokes equation, which highlights the predominance of viscous forces [5, 36]. Under such conditions, flow is termed Stokes flow or creeping flow [2].

$$0 = -\nabla \mathrm{P} + \mu\nabla^2\boldsymbol{u} \tag{15}$$

For 1 < *Re* <100, inertia is finite and plays a role alongside viscous forces [44]; hence, phenomena such as inertial migration and secondary flow emerge [2, 44, 45], although flow is still considered laminar [45].

Inertial migration refers to the lateral movement, perpendicular to the flow direction and across streamlines, of buoyant particles suspended in the channel, after a long enough distance [44, 46, 47]. This phenomenon, uncovered in the 1960s [48], has only found practical use as microfluidic technology developed, as particles with dimension in the order of magnitude of the characteristic dimension of the channel are available [44], and has been at the core of a dedicated field in microfluidics.

Secondary flow can be defined as a marginal flow orthogonal to the primary flow that can be observed in curved channels or in channels with obstacles [44, 49]. The secondary flow assists the inertial migration of particles and alters their final equilibrium position [44, 49]. Briefly, when a fluid flows in a curved channel, the momentum of the fluid elements near the centerline exceeds that of those close to the wall. Hence, due to inertia, the fluid elements with higher momentum move outward and displace the stagnant elements near the wall, which are forced to move

inward. Overall, this results in the formation of two symmetric counter rotating streams, termed Dean vortices or Dean flow, which can be characterized by the Dean number, *De*, of which one common representation is given (Eq. 16) [45, 49, 50].

$$De = \mathrm{Re}\left(\frac{d_h}{2R_c}\right)^2 \tag{16}$$

where R_c stands for the curvature radius of the channel. The velocity of the secondary flow in a Dean vortex can be determined according to Eq. 17 [45].

$$u_{De} = 1.84 \times 10^{-4} De^{1.63} \tag{17}$$

The goal of *De* being to relate the magnitude of transverse flow to longitudinal flow [36], other equations for *De* calculation have been proposed [51]. Irrespectively of such alternate possibilities, a straight channel has an infinite R_c; hence, in such configuration, $De = 0$ [45]. Further details on inertial microfluidics and Dean flow can be found elsewhere [44, 45, 49, 51].

Under the laminar conditions prevailing in microfluidics, mass transfer becomes diffusion-limited, unlike typical macroscopic conditions, where due to the prevalence of inertia and turbulence, convection is typically dominant [2, 37]. Diffusion refers to the thermally induced random molecular movement of the solute (e.g., Brownian motion) downhill a concentration gradient [52–54]. Since in laminar flow fluids flow in parallel layers, mass transport perpendicular to flow and mixing only occurs by diffusion [2]. Convection refers to solute mass transfer through bulk fluid motion and involves the collective displacement of aggregates of solute molecules within fluids [54–56] by combining advection (transport mechanism due to the bulk motion of the fluid) and diffusion [54, 57, 58]. Notwithstanding, the terms advection and convection are often used interchangeably [37, 59, 60].

4 Mass Transport

4.1 Diffusion

The natural migration through a random population of particles from a region of high concentration to a region of low concentration under steady state can be quantified by Fick's first law (Eq. 18) [2, 3, 5]:

$$\boldsymbol{J} = -\boldsymbol{D}\nabla C \tag{18}$$

where $\boldsymbol{J}$ is the diffusive flux vector $\left(\frac{\text{mol}}{\text{m}^2\text{s}}, \frac{\text{kg}}{\text{m}^2\text{s}}\right)$, $\boldsymbol{D}$ is the diffusion coefficient (m^2/s), which shows how fast a solute is dispersed in the medium and can be replaced by a scalar diffusion coefficient, D, assuming that diffusion is isotropic, and ∇C is the concentration gradient ($\text{mol}/\text{m}^3, \text{kg}/\text{m}^3$) [3, 5]. D can be determined experimentally or estimated using suitable correlations [61], of which the most common are the Stokes-Einstein and Wilke-Chang correlations [62]. When diffusion in liquids is considered, D has values in the range of 10^{-9} to 10^{-10} m^2/s, safe for large macromolecules, leading to poorer diffusion [3, 37, 63]. Often, Fick's first law can be reduced to one dimension, leading to Eq. 19.

$$J = -D\frac{dC}{dz} \tag{19}$$

The steady sate only holds if the concentration gradient is preserved, e.g., by continuous feeding and sinking of solute, otherwise it will change over time to yield Eq. 20, known as Fick's second law [64], which shows how the concentration gradient shifts with time at any position [2]:

$$\frac{\partial C}{\partial t} = D\frac{\partial^2 C}{\partial z^2} \tag{20}$$

Solutions for Eq. 20 depend on the boundary conditions [2, 3]. Still, as diffusion in a microfluidic channel is one dimensional, the resulting concentration profile is given by Eq. 21 [3, 64].

$$C = \frac{C_o}{\left(4\pi Dt\right)^{0.5}} e^{\left(-\frac{z^2}{4Dt}\right)} \tag{21}$$

where C_o stands for the initial concentration of the solute (at t = 0 and z = 0). Irrespectively of the boundary conditions used, the term $(4Dt)^{0.5}$, so-called diffusion length δ_l, is found, which establishes how far the concentration has spread in the z-direction [2, 37, 38, 65]. Accordingly, a diffusion time, δ_t, can be defined that relates to the square of the characteristic length, $\delta_t \sim \frac{l^2}{D}$ [36, 37], which highlights that mass diffusion for transport of molecules is only effective for short distances [2].

4.2 Diffusion and Advection

Many real-life situations involving mass transfer rely on the combination of advection and diffusion [66, 67], which can be modeled according to Eq. 22 [37, 68]:

$$\frac{\partial C}{\partial t} + \nabla\left(\boldsymbol{u}C\right) = D\nabla^2 C \tag{22}$$

which may require an extra term on the right-hand side in the case of a source or sink of solute (e.g., chemical reaction) [61].

The relative relevance of advection to diffusion can be determined by the Péclet number (*Pe*) (Eq. 23) [3, 37], where advection considers the average linear velocity and the characteristic dimension perpendicular to the direction of flow and the diffusion coefficient, relates to the molecular transport of the solute [3, 41, 69].

$$Pe = \frac{ul}{D} \tag{23}$$

Naturally, as the dimension of system decreases, *Pe* also decreases, and diffusion tends to gain the upper hand [10]. Hence, given the range of characteristic dimensions of microfluidic devices, diffusion tends to gain relevance in such environments [10]. However, this must be carefully addressed. As several authors point out, a diffusion-controlled system occurs for *Pe* lower than 1 [2, 37]. However, this may not be that common in microfluidics range, at least when liquid handling is envisaged, unless operation is performed under a very low *Re* under a very favorable length to width ratio of the microchannel, but rather in nanofluidics [3, 70].

Overall, *Pe* values largely exceeding 1 can be found in microfluidics; hence, advection may not be fully ruled out [37]. Further illustrative examples and particularly on the relation between *Pe* and *Re* this can be found in dedicated reviews [71, 72]. Actually, and although diffusion-controlled systems are most predictable and easily modeled, purely diffusion mixing, which takes place at the interface of contacting fluid layers, can be a hindrance (e.g., chemical reactions or solute extraction involving two immiscible liquid phases, point-of-care and μTAS systems), as unacceptably long mixing times (e.g., minutes or longer) or otherwise extremely long microchannels may be required [67, 73]. This can also be ascertained if one considers that *Pe* can also be considered as depicting the ratio of diffusion time and convection time, that is, $\frac{l_t^2 / 4D}{l_l / u}$. For disambiguation, characteristic dimension l, is given as either l_t (transversal distance to flow for diffusion) or l_l (longitudinal distance, alongside to flow for convection), e.g., in the specific case of a circular microchannel, $\frac{R^2 / 4D}{l / u}$) [36, 74–78].

Pe number has also been used to esteem the relevance of Taylor diffusion (or Taylor dispersion) in Poiseuille flow [37, 70]. Taylor diffusion consists in the spreading of a solute as it flows along a channel, so that in a broader distribution of the solute along the direction of flow is observed, overall resulting in enhanced dispersion (or diffusion) [70, 78–80], as expressed by the effective diffusivity, D_{ef} (Eq. 24) [81].

$$D_{ef} = D\left(1 + \kappa Pe^2\right) \tag{24}$$

Thus, should $Pe \ll$ length to width ratio of the microchannel, then Taylor dispersion is observed; in contrast, for $Pe \gg$ length to width ratio of the microchannel, then advection is dominant [70].

Advection can be further divided into integrable advection and chaotic advection [82]. The former relates to the regular flow of individual particles in a fluid, so that the dynamical system for the particle trajectories is integrable [83, 84]. The latter refers to the unpredictable and complex trajectories of individual particles in a fluid, so that the trajectory and thus final position of the particle can vastly differ depending on the initial position of the particle [82, 83]. In any case, chaotic advection promotes stretching and folding of material interfaces, the former enlarging the length of the interface and the latter forcing the fluid element to fit in a given region of space. The deformation of fluid boundaries increases the interfacial area available for diffusion, hence mixing is significantly enhanced [85–87].

Chaotic advection differs from turbulent advection as the former results in a time-dependent spatial structure, whereas the latter results in a time- and space-dependent spatial structure [83].

4.3 Mixing

Full mixing, which requires a homogeneous concentration of the mixture can be challenging in microfluidic environments, given the need to effectively combine two fluids under laminar flow with restrictions in space and time [67]. Diffusive mixing featured by laminar flow is often deemed too slow [88], whereas advection is associated with disruptions in the fluid flow [67].

To establish the efficiency of mixing, some form of quantitative measurement is required [89].

In addition to the already mentioned *Re* and *Pe*, Hesel and co-workers also suggest the use of the Fourier number, Fo, a dimensionless time that relates the diffusive mixing time to the residence time and expressed as given in Eq. 25 [90, 91] to determine the mixing efficiency [91, 92].

$$Fo = \frac{Dt}{l^2} = \frac{L/u}{d_h^2/D} \tag{25}$$

These authors further report a relation between mixing length (m_l) and *Pe* under given flow profiles; for example, under laminar, monoaxial flow $m_l \sim Pe \cdot W$, whereas under chaotic advection $m_l \sim \ln(Pe)$ [91].

The use of mixing indices, which are based on the use of mathematical functions over a series of pictures, and mostly rely on the measurement of standard deviation (σ) has been suggested, as exemplified in Eq. 26 [93, 94].

$$\sigma = \left[\frac{1}{N} \sum_{i*1}^{N} \left(i_i - \bar{i} \right)^2 \right]^{0.5} \tag{26}$$

where i_i and $\bar{i}$ stand for the local pixel intensity and the average pixel intensity at the cross-section, respectively, and N stands for the total number of pixels; σ varies within 0 (fully mixed fluids) and 0.5 (fully segregated fluids) and the percent of mixing could be established according to Eq. 27 [94].

$$\text{Mixing} = \left(1 - 2\sigma\right) \times 100 \tag{27}$$

Based on the determination of σ, Huang and co-workers suggested the determination of an average mixing time ($\bar{\tau}_m$) defined according to Eq. 28 [95].

$$\bar{\tau}_m = \frac{L_m}{u} \tag{28}$$

where L_m stands for the distance between segregated and fully mixed regions.

However, σ presents a dimension of intensity, and comparison of mixing extent among different studies is unfeasible [93]. Still, σ can be normalized according to Eq. 29 to deliver an absolute mixing index (ami), which varies from 0 (fully mixed fluids) and 1 (fully segregated fluids) [93, 96].

$$\text{ami} = \frac{\sigma}{\bar{i}} \tag{29}$$

Still, ami only allows for comparison among different studies if either similar lighting conditions or inks are used or complex data processing is used [93]. To overcome this, Hashmi and Xu suggested the use of a relative mixing index (rmi, Eq. 30) that normalizes σ to the unmixed state [93].

$$\text{rmi} = 1 - \frac{\left[\frac{1}{N} \sum_{i*1}^{N} \left(i_i - \bar{i} \right)^2 \right]^{0.5}}{\left[\frac{1}{N} \sum_{i*1}^{N} \left(i_{0i} - \bar{i} \right)^2 \right]^{0.5}} \tag{30}$$

where i_{0i} stands for the local pixel intensity in the unmixed state and rmi of RMI varies from 0 (fully segregated fluids) to 1 (fully mixed fluids). Further information on the quantification of the mixing index can be found elsewhere [97, 98].

Detailed information on the methods used for the visualization and characterization of mixing and flow in microchannels can be found elsewhere [99, 100].

Mixing due solely to diffusion is often far from adequate due to the long mixing times associated [68]. It is known that high aspect ratio microchannels decrease

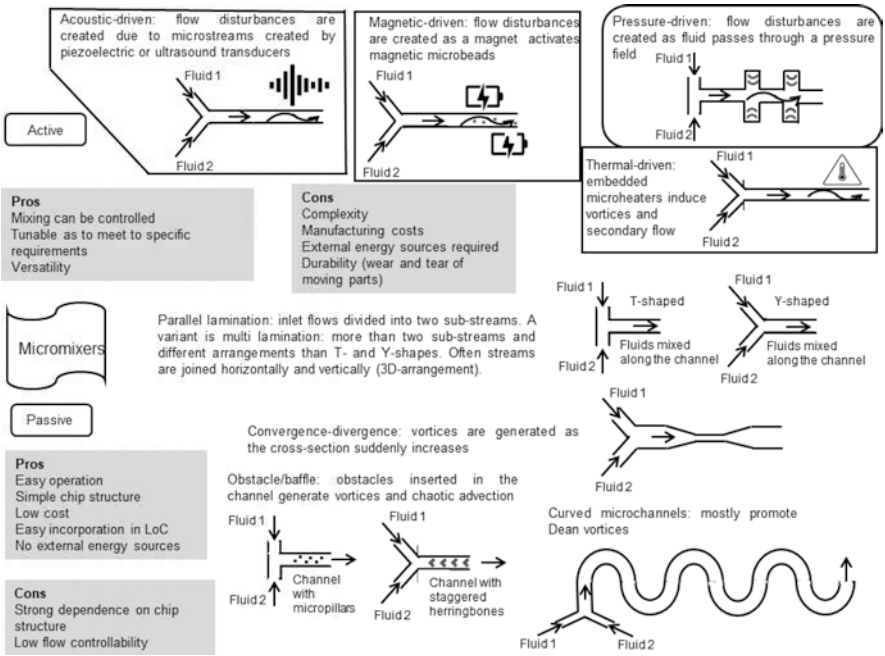

Fig. 3 An overview of micromixers: types, illustrative examples, and main advantages and drawbacks

diffusion path [37, 101], but this is a very restrictive option and even when applicable may not be enough to counter the limitations of diffusion to promote rapid mixing; hence, there is a need for mixers, which introduce chaotic advection and thus maximize the contact area and contact time between mixing species [68].

Several types of mixers have been introduced in microfluidic devices, but they can be ascribed to two groups, active and passive micromixers. The former abridge approaches where an external energy source, e.g., acoustic, magnetic, pressure, or thermal fields, is applied to improve mixing. The latter rely on the proper manipulation of the flow in microchannels using diverse geometric configurations, e.g., baffles and obstacles, curved channels, to improve diffusion and chaotic advection [68, 91, 102]. Detailed insight on micromixers can be found in recently published works [67, 68, 92, 97, 98, 102–105]. Still, a short summary of key aspects of micromixers is given in Fig. 3.

5 Surface Tension

Microfluidic devices often involve two-phase (liquid-liquid/liquid-gas) systems. Moreover, the interaction between the fluid(s) and the container may condition flow behavior. Surface tension plays a significant role when these matters are considered. This section will address relevant aspects associated with the role played by surface tension, in particular the key dimensionless numbers used to characterize the phenomena associated and their significance.

5.1 Capillarity

Capillarity (or capillary action), by definition, refers to the ability of a fluid to move in narrow spaces [106]. Naturally, it is not surprising that capillarity is of most relevance in microfluidics, as it enables to fill microchannels without the aid of external sources/devices [107], which is of relevance for, e.g., assembly of practical point-of-care devices [108]. Capillarity is the result of the action of adhesive and cohesive forces involving fluids and surfaces. Adhesive forces are attractive forces between dissimilar molecules, whereas cohesive forces are attractive forces between similar molecules. For simplicity of further discussion, one may consider the behavior of a liquid contained in a capillary (Fig. 4).

In the interface between the liquid and gas (e.g., air), a meniscus (or curved interface) is typically formed, which is the result of the different energy of the molecules present in the bulk liquid and those in the interface. This forces the surface of the liquid to contract and behave somehow like a stretched membrane. The energy required to increase the surface area by one unit, which can also be interpreted as the tension per unit length required to achieve the same goal, is defined as surface

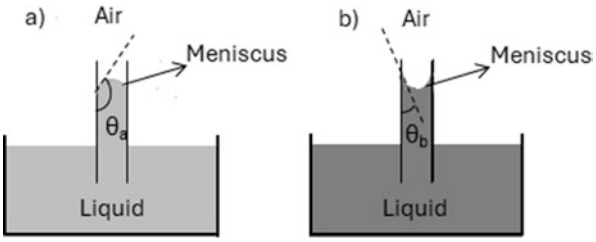

Fig. 4 Schematic of liquids in narrow channels. At the interface between air and liquid, a meniscus is formed. Its orientation—(**a**) convex for the liquid and (**b**) convex for the liquid—depends on the affinity between the fluid and the surface. The contact angle, θ, is the equilibrium of a balance involving the surface tension of the liquid, the surface tension of the solid, and the interfacial tension between the liquid and the solid. In a more practical perspective, θ corresponds to the angle between a tangent to the liquid surface and the solid surface at a given point. Two different angles are depicted, $\theta_a > 90°$, illustrative of poor affinity between the liquid and the surface, opposite to $\theta_b < 90°$, illustrative of good affinity between the liquid and the surface

tension, γ [3, 109]. The curved interface implies a pressure difference between the two adjacent bulk fluid phases, ΔP, which can be related to the curvature radii of the interface, R_1 and R_2, at a given point of the surface of the meniscus, according to Eq. 31, known as Laplace equation [3, 110, 111]:

$$\Delta P = \gamma \left(R_1^{-1} + R_2^{-1} \right) \tag{31}$$

which, e.g., in the case of a sphere [5], where $R_1 = R_2 = R$, is simplified to Eq. 32:

$$\Delta P = 2\gamma R^{-1} \tag{32}$$

Further details on curvature radii can be found elsewhere [111]. On the other hand, one must also consider the interaction between the molecules at the surface and the wall (adhesive forces). Should these exceed the cohesive forces, the liquid will wet the well, and the surface of the liquid close to the wall will be tilted upward. In contrast, should the cohesive forces exceed the adhesive forces, then the surface of the liquid close to the wall will be tilted downward [109, 112]. These situations can be rapidly assessed through the contact angle, θ, which is established between the wall and the tangent to the surface of the liquid where it contacts the wall (Fig. 4) [109, 112]. The contact angle is also useful to classify a surface as either hydrophobic or hydrophilic and, concomitantly, establish the wettability, i.e., the ability of a liquid droplet to spread or not in contact with a solid surface (Fig. 5) [3, 107, 109]. The rise or fall of a liquid column with height H and density ρ within a capillary with radius R can be assessed taking into consideration the surface tension and gravitational effects in the form of a balance of forces (Eq. 33) [37, 106, 109, 111, 112].

Briefly, the liquid will be displaced to a given level until potential energy is balanced by the change of energy of the meniscus (Fig. 6):

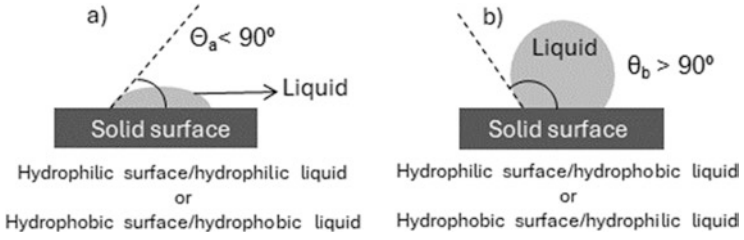

Fig. 5 Assessment of the wettability of a solid surface based on the contact angle. The ability of a liquid to spread over the surface depends on the hydrophilic/hydrophobic nature of liquid and solid. (**a**) Similar nature corresponds to contact angles under 90°, hence suggesting wettability; (**b**) opposite nature corresponds to contact angles over 90°, hence reducing wettability. Patterning the wettability of a surface may be used to move drops [3]

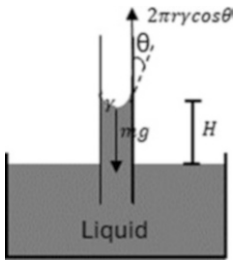

Fig. 6 Illustrative schematics of capillary displacement as a result of the balance between surface tension and gravitational forces

$$ST_v = CW \Leftrightarrow 2\pi R\gamma\cos\theta = mg \Leftrightarrow 2\pi R\gamma\cos\theta = \rho Vg \Leftrightarrow 2\pi R\gamma\cos\theta = \rho\pi R^2 Hg \Leftrightarrow H = \frac{2\gamma}{\rho gR}\cos\theta \Leftrightarrow H = 2l_c^2\ \frac{\cos\theta}{R} \tag{33}$$

where ST_v, CW, and g stand for the vertical component of the surface tension, the column weight, and the acceleration of gravity, respectively, and capillary length can be defined as $l_c = \left(\frac{\gamma}{\rho g}\right)^{0.5}$.

Capillary length illustrates the competition between capillary and gravity and provides an estimate of the relative importance of surface tension and gravity, since if l_c> channel size (e.g., diameter), then gravity is negligible and capillary flow is promoted [3, 5]. Moreover, l_c also provides an estimate for the height of the meniscus [3, 109].

5.2 Surface Tension and Related Dimensionless Numbers

The relevance of surface tension as compared to other effects is established through several dimensionless numbers, namely:

Bond (*Bo*)(or Eötvös, *Eo*) number (Eq. 34)

$$Bo\left(Eo\right) = \frac{\text{gravitacional force}}{\text{surface tension}} = \frac{\rho g l^2}{\gamma} = \frac{l^2}{l_c^2} \tag{34}$$

This relates buoyancy and capillary effects [5, 37, 113–115]. Often ρ may be replaced by $\Delta\rho$, e.g., in multiphase flow where one fluid is embedded in a second fluid [113, 115]. However, when $\Delta\rho$ is small, buoyancy force can be neglected and $Bo \ll 1$ [116]. *Bo* can also incorporate other forces representative of buoyancy, e.g., centrifugal force, where the numerator in Eq. 34 can be given by $\Delta\rho R_c\omega^2 l^2$, where R_c stands for the radius from the center of rotation and ω stands for the rotation speed [117]. *Bo* depends on the square of length scale, and thus minor changes in the characteristic dimension of the channel, e.g., the radius, significantly impacts *Bo*. In microfluidic applications, *Bo* is often noticeably smaller than 1, which

highlights the dominance of surface tension [5, 37, 113, 114]. Moreover, specific ranges of *Bo* have been suggested to label the behavior of multiphase flow [114]. Notwithstanding other situations, *Bo* is particularly useful in the analysis of droplet formation [113, 115, 116].

Capillary number (*Ca*) (Eq. 35)

$$Ca = \frac{\text{viscous forces}}{\text{surface tension}} = \frac{\mu u}{\gamma} \tag{35}$$

This relates viscous and capillary effects (when Eq. 35 is used within the scope of a two-phase system, u typically refers to the dispersed phase [113]). It is generally used to assess how the interface between two fluids, e.g., gas-liquid, two immiscible liquids, is affected by surface tension and viscous forces. The former tend to minimize the surface energy of fluids, e.g., by minimizing the surface area, whereas the latter tend to elongate and drag the interface along the flow direction, thus inducing flow instability that leads to, e.g., local pressure increase and ultimately favoring droplet formation [37, 41, 67, 115]. In microfluidic environments, *Ca* is typically much smaller than 1 (10^{-6} to 10^{-4}) [3]; hence, drops are expected to retain a spherical form [41, 115]. Still, when high viscosity fluids, e.g., silicone, are used, *Ca*~1 can be observed under particular conditions [114]. Additionally, although the length scale is not represented in *Ca*, surface tension gains further predominance over gravity as the cross section of the channel decreases [114]. Under proper conditions in a two-liquid phase system, e.g., proper ratio of flow rates and viscosities, droplets can be generated in a controlled manner for $Ca < 0.1$ [3, 118, 119]. Droplet microfluidics has gained relevance since it allows the generation of monodisperse individualized compartments of a few nanoliters that can be used as discrete (bio) chemical reactors, for cell culture, or for drug development, among others, in a highly controlled manner. Additionally, many experiments can be performed simultaneously without increasing the size of the microfluidic device [10, 118]. Further details on the significance of *Ca* in microfluidics and mechanisms of droplet generation can be found elsewhere [3, 113–115, 118].

Weber number (*We*) (Eq. 36).

$$We = \frac{\text{inertial forces}}{\text{surface tension}} = \frac{\rho u^2 l}{\gamma} \tag{36}$$

This compares inertia and capillarity effects (when Eq. 36 is particularly useful within the scope of a two-phase system, where u typically refers to the dispersed phase [37, 113, 115, 118]). Alternatively, and namely within the scope of droplet generation, *We* can be described as the ratio of kinetic energy and surface energy of a droplet expelled from a nozzle. It has been considered the most relevant dimensionless number within the scope of droplet formation and can be used to establish the onset of droplet formation. Once surpassed the critical *We* in a given process, droplet breakup will take place, although this phenomenon may occur at lower *We*. This renders the critical *We* a sufficient, but not necessary, condition for droplet breakup. The latter solely requires that the energy supplied bests friction losses and

the surface energy of the expelled droplet [120]. Therefore, higher *We* favor droplet breakup and formation of smaller droplets. Still, in many microfluidic devices, *We* is smaller than 1, which is beneath typical critical *We* [37, 120]. Nevertheless, manipulation of channel geometry and/or flow conditions creates conditions for *We* to exceed 1 [37, 120].

A limitation of the *We* is the failure to consider viscous effects, which can be relevant when droplets are generated out of very viscous liquids, e.g., with μ roughly in excess of 10×10^{-3} Pa·s [120]. To account for viscous effects, the Ohnesorge number, *Oh*, can be introduced (Eq. 37):

$$Oh = \frac{\text{viscous forces}}{\text{inertia surface tension}} = \frac{We^{0.5}}{\text{Re}} = \frac{\mu}{\left(\rho l \gamma\right)^{0.5}} \tag{37}$$

which relates the internal viscosity dissipation to the surface tension energy and can assist in determining if droplet will coalesce or not in a given process [3, 114, 115, 120]. *Oh* must be used alongside *We*, since the former does not consider velocity. Low *Oh*, e.g., under 0.1, suggests that added energy is mostly transformed into surface tension energy, favoring droplet formation. On the other hand, as *Oh* increases, viscous dissipation gains relevance since it uses most of the added energy, hence hampering droplet formation [120]. *Oh* has also been used as the basis of empirical correlations to esteem the critical *We* [120, 121].

Table 1 Typical flow regimes in microfluidics [113, 114, 122]

Flow regime	Comment	Schematics
Stratified	Laminar flow. Liquids flow in two layers, usually the heavier liquid in the bottom, the lighter liquid on the top	
Bubbly	$F_{NW} \ll F_W$ Droplets/bubbles with smaller diameters than the microchannel characteristic length are formed	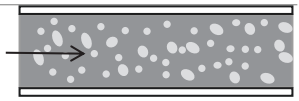
Taylor (slug, segmented)	$F_{NW} \approx F_W$ Slugs/bubbles that occupy most of the cross section of the microchannel. Length of slugs/bubbles affected by inlet features	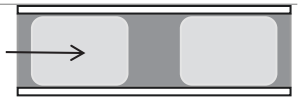
Annular	$F_W/F_{NW} \ll 1$ Wetting phase flows close to the wall, as an annular film (in circular cross-section microchannels) or with various thicknesses along the perimeter for other microchannel geometries	
Churn	Very high velocities lead to chaotic flow leading to irregularly shaped droplets and bubbles	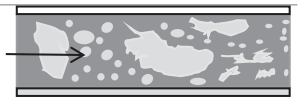

F_W Flow rate of wetting phase, F_{NW} Flow rate of non-wetting phase